IEEE.org | IEEE Xplore | IEEE SA | IEEE Spectrum | More Sites SUBSCRIBE Cart Create Account | Personal Sign In

IEEE Xplore® Browse My Settings Help Institutional Sign In IEEE

All

ADVANCED SEARCH



# Self-Adaptive Fuzzy Control Approach for Jack-up Rig Jacking System Based on Particle Swarm Optimization

**Publisher: IEEE**

Cite This PDF

Xuan-Kien Dang ; Tien-Dat Tran ; Viet-Dung Do ; Le Anh-Hoang Ho ; Van-Vang Le All Authors

31 Full Text Views

Open Access Comment(s)

Need Full-Text access to IEEE Xplore for your organization? CONTACT IEEE TO SUBSC PDF Help

More Like This Feedback



**Abstract:**

Many offshore projects, such as offshore oil and gas exploration and offshore wind farm development, have required controlling the position of elevating the hull in a stable and balanced manner in recent years. The Jack-up Rig (JuR) jacking control systems are a revolutionary innovation that is already being employed in offshore drilling and other maritime structures. The system is utilized automatically to control and stabilize the position of the JuR during sea state disturbances to keep platforms from being displaced. As a result, developing an improved control theory for the Jacking system (JS) of a JuR is very important. In this paper, first, we investigate how to adapt to the effects of external forces and hydrodynamic amplification using a particle swarm optimization strategy based on a fuzzy controller. Then, using the fuzzy controller as the foundation, we proposed the PSO - Self Adaptive Fuzzy Controller (PSO-SAFC) guaranteed by Lyapunov criteria and compares it with other fuzzy-based algorithms to show the benefit of adaptively and stability of the system. To verify the proposed algorithm, embedded STM32F746VG central processor used to build the algorithm and run Simulink models on Matlab, the collected data on the positions of the legs and the tilt compared it to the setting command values to move the Rig body and provided control signals to the Drive system. Eventually, the advantages of the proposed approach are demonstrated by the simulation and experiment outcomes.

**Published in:** IEEE Access ( Volume: 10)

**Page(s):** 86064 - 86077 **INSPEC Accession Number:** 22008832

**Date of Publication:** 10 August 2022 **DOI:** 10.1109/ACCESS.2022.3197835

**Electronic ISSN:** 2169-3536 **Publisher:** IEEE

**Funding Agency:**

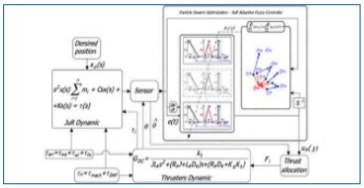

Proposed PSO - self adaptive fuzzy controller structure.

algorithms

Proceedings of the 10th World Congress on Intelligent Control and Automation

Published: 2012

PDF Help

Particle swarm optimization fuzzy supervisory controller for nonlinear position control system

2013 8th International Conference on Computer Engineering & Systems (ICCES)

Published: 2013

Show More

IEEE iapp

Get Critical Training Feedback

Get Critical Training on Privacy by Design for Engineers

LEARN MORE >

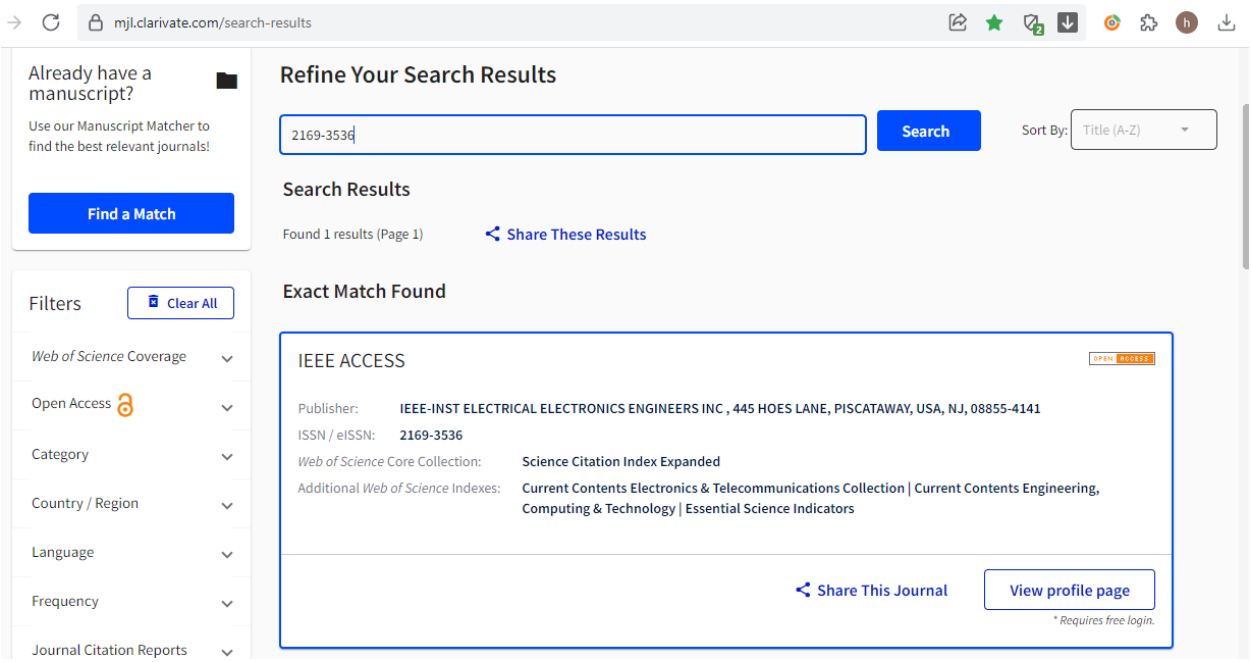
mjl.clarivate.com/search-results
Already have a manuscript?
Use our Manuscript Matcher to find the best relevant journals!
Find a Match
Refine Your Search Results
2169-3536
Search
Sort By: Title (A-Z)
Search Results
Found 1 results (Page 1)
Share These Results
Filters
Clear All
Web of Science Coverage
Open Access
Category
Country / Region
Language
Frequency
Journal Citation Reports
Exact Match Found
IEEE ACCESS
Publisher: IEEE-INST ELECTRICAL ELECTRONICS ENGINEERS INC , 445 HOES LANE, PISCATAWAY, USA, NJ, 08855-4141
ISSN / eISSN: 2169-3536
Web of Science Core Collection: Science Citation Index Expanded
Additional Web of Science Indexes: Current Contents Electronics & Telecommunications Collection | Current Contents Engineering, Computing & Technology | Essential Science Indicators
Share This Journal
View profile page
* Requires free login.

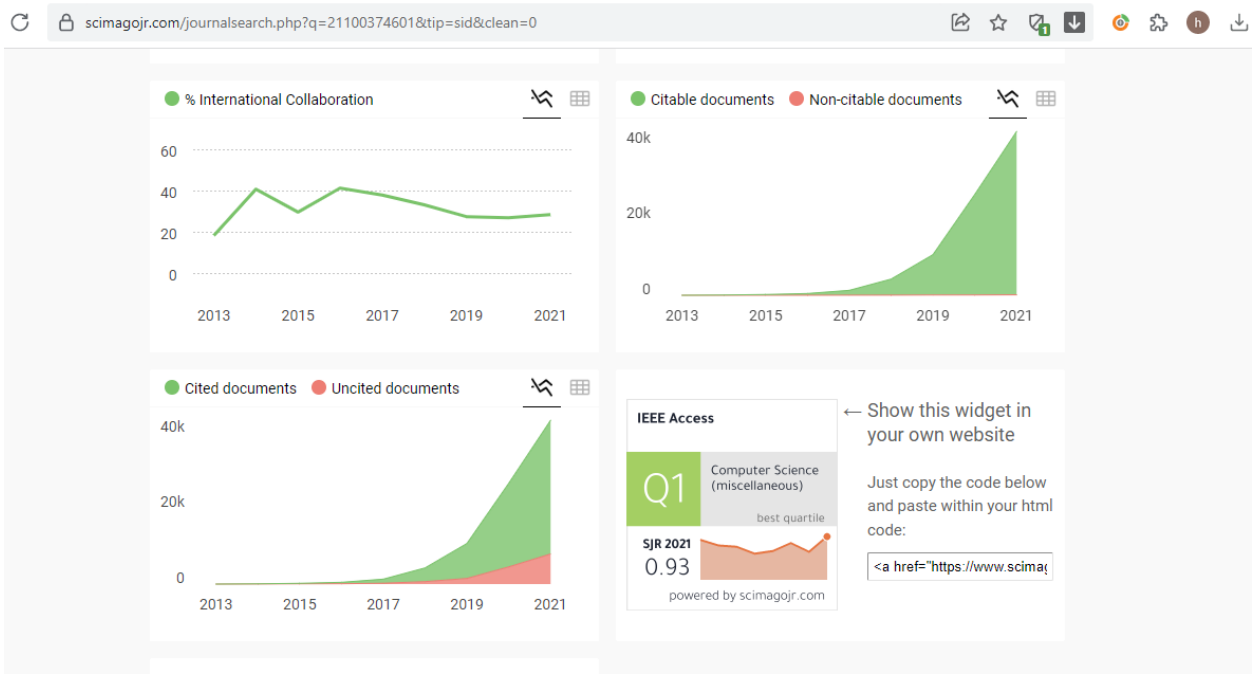
scimagojr.com/journalsearch.php?q=21100374601&tip=sid&clean=0
% International Collaboration
60
40
20
0
2013
2015
2017
2019
2021
Citable documents
Non-citable documents
40k
20k
0
2013
2015
2017
2019
2021
Cited documents
Uncited documents
40k
20k
0
2013
2015
2017
2019
2021
IEEE Access
Q1
Computer Science (miscellaneous)
best quartile
SJR 2021
0.93
powered by scimagojr.com
← Show this widget in your own website
Just copy the code below and paste within your html code:
<a href="https://www.scima

IEEE Access
Multidisciplinary | Rapid Review | Open Access Journal

Received 27 June 2022, accepted 5 August 2022, date of publication 10 August 2022, date of current version 22 August 2022.

*Digital Object Identifier 10.1109/ACCESS.2022.3197835*

RESEARCH ARTICLE

# Self-Adaptive Fuzzy Control Approach for Jack-up Rig Jacking System Based on Particle Swarm Optimization

**XUAN-KIEN DANG[1], (Member, IEEE), TIEN-DAT TRAN[1], (Member, IEEE), VIET-DUNG DO[1,2], (Member, IEEE), LE ANH-HOANG HO[1,3], AND VAN-VANG LE[1]**

[1]Artificial Intelligent in Transportation, Ho Chi Minh City University of Transport, Ho Chi Minh City 700000, Vietnam
[2]Dong An Polytechnic, Di An, Binh Duong 75000, Vietnam
[3]Faculty of Engineering and Technology, Van Hien University, Ho Chi Minh City 700000, Vietnam

Corresponding author: Xuan-Kien Dang (dangxuankien@hcmutrans.edu.vn)

This study was supported by the Research Program of Transport Ministry of Vietnam under Grant DT223013 (2022).

**ABSTRACT** Many offshore projects, such as offshore oil and gas exploration and offshore wind farm development, have required controlling the position of elevating the hull in a stable and balanced manner in recent years. The Jack-up Rig (JuR) jacking control systems are a revolutionary innovation that is already being employed in offshore drilling and other maritime structures. The system is utilized automatically to control and stabilize the position of the JuR during sea state disturbances to keep platforms from being displaced. As a result, developing an improved control theory for the Jacking system (JS) of a JuR is very important. In this paper, first, we investigate how to adapt to the effects of external forces and hydrodynamic amplification using a particle swarm optimization strategy based on a fuzzy controller. Then, using the fuzzy controller as the foundation, we proposed the PSO - Self Adaptive Fuzzy Controller (PSO-SAFC) guaranteed by Lyapunov criteria and compares it with other fuzzy-based algorithms to show the benefit of adaptively and stability of the system. To verify the proposed algorithm, embedded STM32F746VG central processor used to build the algorithm and run Simulink models on Matlab, the collected data on the positions of the legs and the tilt compared it to the setting command values to move the Rig body and provided control signals to the Drive system. Eventually, the advantages of the proposed approach are demonstrated by the simulation and experiment outcomes.

**INDEX TERMS** Adaptive robust control, dynamic positioning, environmental loads, jacking control, rig move.

## I. INTRODUCTION

### A. BACKGROUND

Offshore oil and gas exploration, drilling, and work-over have all been done on jack-up drilling platforms for decades. In the jacking operation of a JuR, there are numerous approaches [1], [2], [3], [4] for ensuring stable control and reducing influencing forces (JuR) to the process. Even if each technique has its own set of advantages, the study of advanced control algorithms pushes researchers to develop theory and practice solutions to help the system work more consistently and securely control system and has many more operations than before.

The JuR is a kind of movable platform consisting of a large floating hull outfitted with multiple detachable legs, usually three or four, capable of elevating the hull above the sea's surface [3], [4]. The 3-legs JUR 3D-designed model shown in Fig. 1, for example, are triangular barges that have been completely fitted during the drilling process and are motivated by three truss legs, the other shapes are utilized less frequently due to their complexity in structure and organization. JuR is also known for developing the jacking control system, which

The associate editor coordinating the review of this manuscript and approving it for publication was Yanli Xu.


This work is licensed under a Creative Commons Attribution 4.0 License. For more information, see https://creativecommons.org/licenses/by/4.0/

**TABLE 1. List of abbreviation.**

| Number | List | |
|---|---|---|
| | Abbreviation | Description |
| 1 | JuR | Jack-up Rig |
| 2 | JuRs | Jack-up Rigs |
| 3 | PSO | Particle Swarm Optimization |
| 4 | AFC | Adaptive Fuzzy Control |
| 5 | FC | Fuzzy Control |
| 6 | FPSO | Fuzzy Particle Swarm Optimization |
| 7 | PID | Proportional Integral Derivative |
| 8 | FPID | Fuzzy Proportional Integral Derivative |
| 9 | SAFC | Self-Adaptive Fuzzy Control |
| 10 | JS | Jacking System |
| 11 | JSs | Jacking Systems |
| 12 | GA | Genetic Algorithm |
| 13 | ACO | Ant Colony Optimization |
| 14 | CMAC | Cerebellar Model Articulation Controller |
| 15 | PSO-SAFC | PSO - Self Adaptive Fuzzy Controller |
| 16 | DAF | Dynamic Amplification Factor |
| 17 | SDOF | Single Degree of Freedom |
| 18 | MFs | Membership Functions |

**TABLE 2. Nomenclature.**

| DESCRIPTION | SYMBOL | UNIT |
|---|---|---|
| Damping | $C$ | |
| Stiffness | $K$ | $N/m$ |
| Overall torque of motors | $\tau_m(t)$ | $Nm$ |
| Wave impact factor | $\tau_{wa}(t)$ | |
| Win impact factor | $\tau_{wi}(t)$ | |
| Current impact factor | $\tau_{cu}(t)$ | |
| Damping ratio | $\zeta$ | |
| Angular velocity of gear | $\omega_n$ | $rad/s$ |
| Revolutions per minute of gear | $n$ | $rpm$ |
| The actual position of the hull | $x$ | $m$ |
| Gear radius | $R$ | $m$ |
| The number of teeth | $z$ | |
| The module | $m$ | $mm$ |
| Gear rotation angle | $\theta(s)$ | $deg$ |
| The length of the cylindrical element generatrix | $L$ | $mm$ |
| The tolerances of cylindricity | $t_{cy}$ | $mm$ |
| Conversion factor | $k_e$ | |
| Maximum clearance | $\Delta_J$ | $mm$ |
| Rotation angle error caused by clearance | $\theta_a$ | $arc\ min$ |
| The clearance-induced rotation errors of the gear axis around the x- and y-axes | $\theta_{Jx}, \theta_{Jy}$ | $mm$ |
| Rotation angle error due to tooth pitch error | $\Delta p_k$ | $arc\ min$ |
| Individual tooth pitch deviation | $\Delta f_{pt}$ | $\mu m$ |
| Limit deviation of individual tooth pitch | $f_{pt}$ | $\mu m$ |
| Phase angle of eccentric assembly | $\gamma$ | $(0-2\pi)$ |
| Wave direction | $\psi_r$ | $deg$ |
| The wave spectrum | $S$ | |
| The phase angle of wave components | $\phi_{qr}$ | $(0-2\pi)$ |
| The harmonic amplitudes of wave frequency | $\Delta\omega, \Delta\psi$ | |
| Wave frequency | $\omega_q$ | $Hz$ |
| The number of waves | $k_q$ | |
| Wavelength | $\lambda_q$ | $m$ |
| The density of air | $\rho_\omega$ | $kg/m^3$ |
| Wind direction | $g_R$ | $deg$ |
| Wind speed | $V_R$ | $m/s$ |
| The transverse and lateral projected areas | $A_T, A_L$ | $m^2$ |
| The wind traction | $C_X, C_Y$ | |
| The current speed | $V_c$ | $m/s$ |
| Sideslip angle | $\beta_c$ | |
| The current velocity compositions | $u_C, v_c$ | $m/s$ |
| The angular compositions impacted by high and low frequency | $\psi_L, \psi_H$ | $deg$ |
| Armature inductance | $L_a$ | $H$ |
| Viscous friction constant | $D_a$ | $Nm/rad$ |
| Back emf constant | $K_b$ | $Vs/rad$ |
| Armature resistance | $R_a$ | $\Omega$ |
| Torque constant | $K_t$ | $Nm/A$ |
| Rotor inertia | $J$ | $Kgm^2$ |

has three, four, six, and eight movable legs that can extend upward or below the hull. However, according to recent studies on the laboring environment, the JuR can drill in waters up to 350 feet deep, but for deep water less than 600 feet deep, the overall economics and operational efficiency of deep-water JuRs are typically more favorable than shallow water semi-submersibles [5], [6], [7], [8]. In the conception of jack-up and semi-submersible rigs, the JuR will always be preferred over a semi-submersible rig providing both are capable of digging the well.

Many different types of offshore platforms have been developed depending on a variety of variables, including technical and scientific advancements, economics, the need to use deeper natural resources [9], [10], and disturbance limits [11]. Offshore solutions for the challenges include developing more high-speed technology and conducting more strong study efforts [12], [13], [14], whereas they need more costly expenditures and system design adjustments. Meanwhile, these solutions may be switched by content economically and task methodologies that can be maintained constant at the same time for cost savings, while still utilizing the same system architecture and meeting standards and laws. Offshore engineering has recently received extensive attention from intellectual and industrial researchers to assist service providers and technology suppliers satisfy the high demand requirements for an offshore platform [15], [16]. Just developed systems must eventually assure that human, marine, and coastal ecosystems are safe, while also maintaining the significant time and resource expenditures made.

### B. LITERATURE REVIEW

As can be seen, there are many challenges related to the JuR model, methodologies, and applications, as well as financial concerns, but they all revolve around two questions: 1) which system metrics should be improved (quality, unit cost, scheduling, hourly rate, safety, communication, and technology) and 2) which solutions should be used to ensure JuRs working in a rough environment while keeping operation and maintenance costs as low as possible [17]. Jacking systems (JSs) were designed as vertical transit vehicles to make it easier for the Rig body to go from one level to another by lowering the time it takes to move and the amount of physical energy in the sea. The system is synchronously controlled by the drives attached to the Rig's legs, much the same as heavy lifting equipment. It consists of sets of motors installed together to drive coaxially while simultaneously moving the whole Rig's body in various condition operating modes. In reality, in the field of marine science, various control systems have been investigated to improve system quality [18], assure safety in difficult situations [19], and save energy [20]. Because of the similarities in nature, we can apply a lot of new ideas to the JS if we consider

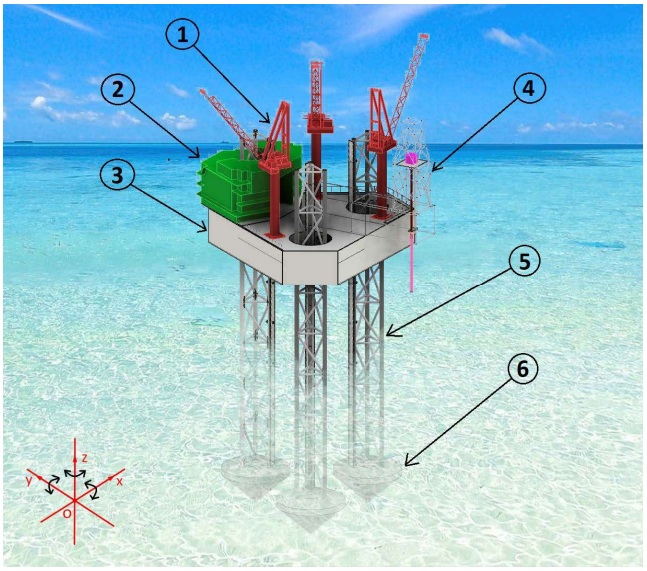


**FIGURE 1.** 3D design model of jack-up rig (1. Crane; 2. Operation area; 3. Flooring; 4. Drilling tower; 5. Rig legs; 6. Spudcans).

it as an elevator system. Only one word of caution: the Rig is huge, has high inertia, and operates in harsher conditions than land-based elevators. Accordingly, with such qualities in mind, this work focuses on challenges relating to fuzzy logic adaptive control, in which the Particle Swarm Optimization (PSO) algorithm is used as a form of artificial intelligence to improve the automatic control adaption capability of fuzzy controllers.

#### 1) SELF-ADAPTIVE FUZZY CONTROL (SAFC)

Nonlinear adaptive control has been studied for several years to deal with the difficulty of uncertainties and disruptions [18], [21], [22], [23]. An improved evolutionary algorithm based on fuzzy logic which is a dynamic multi-objective evolutionary method based on fuzzy logic is described in [24]. When an environmental change happens, it is critical to provide a real and truthful reaction to the change to enhance the variety of options. Robust adaptive control is presented as the best approach for reducing the influence of error and uncertainty disturbance and noise. Therefore, the efficiency of a robust adaptive control employing a bounded estimates scheme of the disturbance by using Genetic algorithm (GA), and the tracking performance with robustness is maintained [18]. In conventional control theory, Lyapunov-based approaches have long been utilized to build controllers that assure the system's closed-loop stability. Tracking the reference input takes a large amount of time using a Lyapunov-based approach, and the inherent approximation error leads the system to have larger integral absolute errors [25]. Thus, adaptive control Lyapunov-based approach appreciate on JS control because this system controls the slow speed with large inertia. Moreover, several existing adaptive fuzzy controllers [26], [27] have a key limitation in that they were designed for systems with limitless actuators. As a result, it can be determined that the SAFC based on Lyapunov criteria always maintains stability under actual conditions and assumptions, and thus the Adaptive fuzzy control (AFC) based on Lyapunov is regarded as viable when the control object is JS.

#### 2) PARTICLE SWARM OPTIMIZATION (PSO)

The optimization of fuzzy systems has received a bit of attention in the recent literature. Optimization algorithms can tackle nonlinear, well-constrained, and even NP-hard problems, making them a powerful tool. Genetic Algorithms [18], Ant Colony Optimization (ACO) algorithms [28], Cerebellar Model Articulation Controller (CMAC) [29], and PSO [21], [28], for example, are among the most widely used optimization approaches. Especially, PSO is a novel evolutionary optimization approach that is rapid, easy, and likely to be utilized for searching a large search space for the optimal answer. Unlike other heuristic strategies, it features a versatile and well-balanced method to boost global and local exploration skills. Furthermore, specifying the target function and placing indefinite boundaries on the optimized parameters is sufficient, and PSO has proven to be successful in many applications when combined with fuzzy logic or artificial intelligence.

#### 3) HYBRID CONTROL APPROACH

Hybrid Control approach focused on a combination of a Lyapunov-theory-based technique and a PSO based optimization approach for developing stable adaptive fuzzy controllers [30], [31], [32] which a potential research direction. The goal is to create a SAFC by optimizing both its structure and parameters such that the controller can ensure necessary stability while also providing sufficient performance. To establish stable Fuzzy control (FC) and assure faster convergence, a Lyapunov-based technique is used in conjunction with PSO. Therefore, we may predict that combining PSO and SAFC approaches will result in a hybrid algorithm that is more efficient.

### C. CONTRIBUTION

To overcome the aforementioned problems, we present a novel model of the PSO - Self adaptive fuzzy controller (PSO-SAFC) to cope with position control for a JS of the JuR. The contributions of the paper are presented as follows:

1. The PSO-SAFC model is proposed with the goal of adapting to external forces, hydrodynamic amplification, and mechanical errors. The PSO algorithm is used to construct the optimal coefficient $\lambda_i$ to enhance the membership function of the fuzzy controller used to increase control quality in a time-varying environment, which is represented in a novel algorithm.

2. A simulation experiment with two case studies compares the FC, AFC, FPID, and PSO-SAFC guaranteed by Lyapunov criteria to demonstrate the benefit of the recommended approach under the influence of uncertain factors.

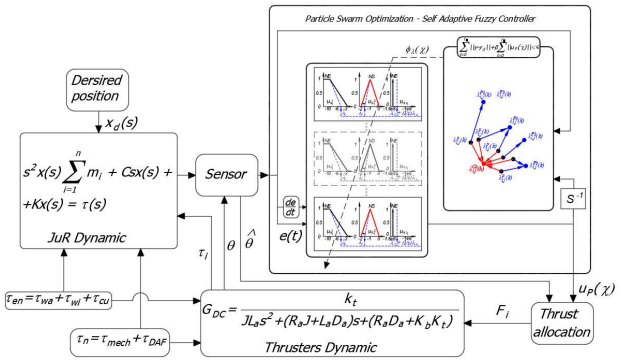


**FIGURE 2.** Proposed PSO - self adaptive fuzzy controller structure.

3. The control algorithm is embedded in the STM32F746-VG central processor with Matlab software, which gathers data on leg locations and rig body tilt and compares it to command values to move the Rig body and generate control signals to the Drive system. Thus, the advantages of the proposed approach are demonstrated by the simulation and experiment outcomes.

The rest of the paper is organized as follows. Section II presents a problem description and motivation. Section III presents the proposed a SAFC by PSO, a Lyapunov based technique is used in conjunction with PSO such that the controller can ensure necessary stability, while in Section IV, simulation and experimental case studies for both conventional FPID, FC, AFC and proposed PSO-SAFC are demonstrated. Section V concludes the paper.

## II. PROBLEM FORMULATION

### A. DYNAMIC EQUATIONS OF JACKING SYSTEM

Figure 1 depicts the hull's motions as well as the relationship of forces. The hull vibrates vertically and horizontally around the X- and Y-axes, moving up and down in the Z-direction. The hull is driven by electric motors positioned on three points on the hull that correspond to the position of the legs in elevating mode. In working conditions, the motors on each position have always had the identical properties and are synchronously controlled at the same speed. Figure 2 shows a schematic of the JS.

The elevating mechanism is used to move the hull to a fixed position. According to the overall diagram in Fig. 2, the force elements pushing on the JuR's hull are determined in the system of differential equations defining the kinematics as follows [33]:

$$M\frac{d^2x(t)}{dt^2} + C\frac{dx(t)}{dt} + Kx(t) = \tau(t) \tag{1}$$

where $M = \sum_{i=1}^{n} m_i$ is total weight of the JuR; $C$, $K$ are damping and stiffness of the system, and $\tau(t) = \tau_m(t) + \tau_d(t)$, $\tau_m(t) = \sum_{i=1}^{n} \tau_i(t)$ is overall torque of motors.

In addition, wave, wind, current, and external noise components are included in the total of the influences of external and internal disturbances. The following is the definition of the equation:

$$\tau_d(t) = \tau_{\mathrm{wa}}(t) + \tau_{\mathrm{wi}}(t) + \tau_{cu}(t) + \tau_n(t) \tag{2}$$

### B. DYNAMIC AMPLIFICATION FACTOR IN TRANSFER FUNCTION OF KINEMATICS OF JS

In general, there are always factors that create fluctuations in actuality. In which, deviations owing to oscillations relating to Dynamic Amplification Factor (DAF) values would impact the actual position in control process of the JS [34].

*Assumption 1:* The JS of the JuR is an Single Degree of Freedom (SDOF) system in elevating mode.

Then, the displacement *DAF* of a damped JS subjected to a step load is consequently calculated as the ratio of the dynamic response to the static response. There are always factors that create fluctuations in actuality. As a result, deviations owing to oscillations relating to *DAF* values would impact the actual position of the hull.

$$x(t) = DAF.x_p(t) \tag{3}$$

The dynamic response of damped JS can be determined based on the Duhamel's integral as

$$x(t) = \frac{\tau(t)}{k}\left[1 - \mathrm{e}^{-\zeta\omega_{\mathrm{n}}t}\left(\cos\omega_{\mathrm{n}}\sqrt{1-\zeta^2}t + \frac{\zeta\sin\omega_{\mathrm{n}}\sqrt{1-\zeta^2}t}{\sqrt{1-\zeta^2}}\right)\right] \tag{4}$$

where $\zeta = (0.05 - 0.2)$ is the damping ratio of the system. Define *DAF* as the ratio of the dynamic response to the static response, the displacement *DAF* of an damped SDOF system subjected to a step load is therefore [35]:

$$\begin{aligned} DAF(t) &= \frac{x(t)}{x_p(t)} \\ &= 1 - \mathrm{e}^{-\zeta\omega_{\mathrm{n}}t}\left(\cos\left[\omega_{\mathrm{n}}\sqrt{1-\zeta^2}t\right] + \frac{\zeta\sin\left[\omega_{\mathrm{n}}\sqrt{1-\zeta^2}t\right]}{\sqrt{1-\zeta^2}}\right) \end{aligned} \tag{5}$$

*Remark 1:* Following Society of Naval Architects and Marine Engineers [34], in case of the Rigs have Mass $>$ 2500*Ton* we have conditions $\zeta < 0.07$ and $t > 0.124$.

*Assumption 2:* In the case of Assumption 1 is satisfied, the *DAF* is bounded in range of $0 < DAF < 2$.

In this study, using Matlab to calculate the *DAF* values that satisfy the conditions in Remark 1 along with Assumption 1 and Assumption 2, we get the results as shown in Table 3, in which $\omega_n = \pi n/30 = 48,984(rad/s)$. Therefore, the selected optimum value of *DAF* is 0.6284 satisfied conditions in Remark 1. Thus, this value will be used to calculated a transfer function of kinematics of JS.

For convenience and simplicity in embedded control and simulation, we use the method of decoupling system to

**TABLE 3.** The calculated values of DAF.

| DAF | t | | | | | | | |
|---|---|---|---|---|---|---|---|---|
| $\zeta$ | 0.025 | 0.05 | 0.075 | 0.10 | 0.125 | **0.15** | 0.175 | 0.20 |
| **0.05** | 0.6352 | 1.6509 | 1.7400 | 0.8985 | 0.2802 | **0.6284** | 1.3986 | 1.5843 |
| 0.075 | 0.6230 | 1.5966 | 1.6866 | 0.9326 | 0.3865 | 0.6726 | 1.3059 | 1.4636 |
| 0.1 | 0.6112 | 1.5454 | 1.6373 | 0.9623 | 0.4781 | 0.7108 | 1.2320 | 1.3680 |
| 0.15 | 0.5886 | 1.4513 | 1.5495 | 1.0097 | 0.6251 | 0.7734 | 1.1268 | 1.2312 |
| 0.175 | 0.5778 | 1.4081 | 1.5102 | 1.0282 | 0.6839 | 0.7994 | 1.0903 | 1.1827 |
| 0.2 | 0.5673 | 1.3672 | 1.4735 | 1.0437 | 0.7347 | 0.8227 | 1.0619 | 1.1438 |

separate the system into subsystems with the same transfer function. Then, substituting $DAF = 0.6284$ into an eq. (3), we have $x(t) = 0.6284x_p(t)$, $\dot{x}(t) = 0.6284\dot{x}_p(t)$, $\ddot{x}(t) = 0.6284^2\ddot{x}_p(t)$. Therefore, eq. (1) is rewritten as

$$0.6284^2M\ddot{x}_p(t)+0.6284C\dot{x}_p(t)+0.6284Kx_p(t) = \tau(t) \quad (6)$$

Using Laplace transform to eq. (6) with initial conditions $x(0) = 0, \dot{x}(0) = 0$, we get

$$0.6284^2Ms^2x_p(s) + 0.6284Csx_p(s) + 0.6284Kx_p(s) = \tau(s) \quad (7)$$

The displacement of the hull is calculated by

$$x_p(s) = R\theta(s) \quad (8)$$

Substituting eq. (8) into eq. (7), we have

$$0.6284^2Ms^2\theta(s) + 0.6284Cs\theta(s) + 0.6284K\theta(s) = k_e\tau(s) \quad (9)$$

with $k_e = 1/R$ is the inverted factor in rotary – translational drive (including the number of motors and transmission coefficients). Finally, the equation describing the transfer function of kinematics of JS is written as:

$$G_{JuR} = \frac{\theta(s)}{\tau(s)} = \frac{k_e}{0.6284^2Ms^2 + 0.6284Cs + 0.6284K} \quad (10)$$

## III. ANALYSIS NEGATIVELY FACTORS EFFECTING ON CONTROL PROCESS

### A. EXTERNAL FACTORS

When the sea state is rough, the JuR is normally not allowed to operate. As a result of the influence of environmental force vectors such as wave, wind, and current force, termed $F_{envi}$ by Fossen *et al.* [36], and Dang *et al.* [18], JS operations are only possible when the sea conditions are calm.

$$F_{envi} = F_{wave} + F_{wind} + F_{current} \quad (11)$$

Waves are the most significant indication of the effect on offshore constructions. In six degrees of freedom, waves force an offshore structure to surge, pitch, roll, sway, heave, and yaw. The $F_{wave}$ wave force equation for the control issue [36] is as follows:

$$\begin{aligned} F_{wave} &= \zeta(x,\ y,\ t) \\ &= \sum_{q=1}^{N}\sum_{r=1}^{M}\sqrt{2S(\omega_q, \psi_r)\Delta\omega\Delta\psi}\,sin(\omega_q t \ldots \\ &\quad \ldots + \phi_{qr} - k_q(xcos\psi_r + ysin\psi_r)) \end{aligned} \quad (12)$$

with $\phi_{qr} \in (0{-}2\pi)$ is the phase angle of wave components. S is the wave spectrum, $\psi_r$ is the direction wave. The $\Delta\omega$ and $\Delta\psi$ is the harmonic amplitudes of wave frequency $\omega_q$. The $k_q = 2\pi/\lambda_q$ is the number of waves, in which $\lambda_q$ is the wavelength.

Wind loads are calculated using one of four methods: wind tunneling, numerical modeling, formulae based on experience, and field testing. The wind force is estimated using the formula [36] with a calm sea state and the system functioning in the condition that the wind frequency and direction are simulated as slowly changing values.

$$\begin{aligned} F_{wind} &= [X_{wind}, Y_{wind}]^T \\ X_{wind} &= 0.5C_X g_R \rho_w V_R^2 A_T \\ Y_{wind} &= 0.5C_Y g_R \rho_w V_R^2 A_L \end{aligned} \quad (13)$$

where $g_R$ is wind direction, $V_R$ is wind speed. $A_T$ and $A_L$ are the transverse and lateral projected areas, represented by $C_X$ and $C_Y$.

Even though the current velocity fluctuates with time, space, depth, and vortex vibration, the current is considered stable. We need to compute the velocity and velocity profile of the flow on the water if we ignore the following elements in the calculation procedure for offshore works. The current velocity is below

$$\begin{aligned} u_c &= V_c cos\,(\beta_c - \psi_L - \psi_H) \\ v_c &= V_c sin\,(\beta_c - \psi_L - \psi_H) \\ F_{current} &= [u_c, v_c, 0]^T \end{aligned} \quad (14)$$

where $u_c$ and $v_c$ are current velocity compositions, and $\psi_L$ and $\psi_H$ are angular compositions impacted by high and low frequency values, respectively. In this study, the simulation would be used to investigate the effects of environmental factors while referencing the parameter Table 5 [21] under suitable weather situations.

### B. MECHANICAL ERRORS

The rack-gear system that raises and lowers the JuR is a cultivated elastic mechanical system that produces vibration and noise. The following sorts of defects can occur in a simple gear system: contact position error, bearing assembly error, axial error, pitch error, and gear radial error.

#### 1) FORM AND POSITION ERRORS

The accompanying is the deviation of geometric components of parts due by cylindricality error: Small translation and rotation error variation ranges are as $(\frac{-t_{cy}}{2}, \frac{t_{cy}}{2})$ and $(\frac{-t_{cy}}{2L}, \frac{t_{cy}}{2L})$, respectively. $L$ is the length of the cylindrical element generatrix, and the error component is expressed as follows [37]:

$$\begin{aligned} &(dx_{cy}, dy_{cy}, dz_{cy}, \delta x_{cy}, \delta y_{cy}, \delta z_{cy}) \\ &\qquad = (dx_{cy}, dy_{cy}, 0, \delta x_{cy}, \delta y_{cy}, 0) \end{aligned} \quad (15)$$

#### 2) COMPOSITION OF GEOMETRIC ERRORS

If several geometric faults impact a part, the total error components are overlaid by each error, therefore

$$\begin{aligned}&(\Delta x_{0i}, \Delta y_{0i}, \Delta z_{0i}, \Delta\partial_{0i}, \Delta\beta_{0i}, \Delta\gamma_{0i})\\&= \begin{pmatrix} dx_{i1} + dx_{i2} + \cdots, d\ y_{i1} + dy_{i2} + \cdots \\ dz_{i1} + dz_{i2} + \cdots, \delta x_{i1} + \delta x_{i2} + \cdots \\ \delta y_{i1} + \delta y_{i2} + \cdots, \delta z_{i1} + \delta z_{i2} + \cdots \end{pmatrix}\\&= \begin{pmatrix} \sum_{j=1}^{n} dx_{ij}, \sum_{j=1}^{n} dy_{ij}, \sum_{j=1}^{n} dz_{ij} \\ \sum_{j=1}^{n} \delta x_{ij}, \sum_{i=1}^{n} \delta y_{ij}, \sum_{i=1}^{n} \delta z_{ij} \end{pmatrix}\end{aligned} \tag{16}$$

where: $dx_{ij}$, $d\ y_{ij}$, $d\ z_{ij}$, $\delta x_{ij}$, $\delta y_{ij}$, $\delta z_{ij}$ are the *jth* error of the *ith* part, respectively. The displacement errors corresponding to the three rotation errors of the same portion under overlapping are given by $\Delta x_{0i}$, $\Delta y_{0i}$, $\Delta z_{0i}$, $\Delta\partial_{0i}$, $\Delta\beta_{0i}$, $\Delta\gamma_{0i}$.

#### 3) AXIAL RUNOUT

Axial runout can be caused by the clearance between the inner bore and the shaft, resulting in transmission problems. Furthermore, a specific amount of clearance is allocated in the design of gear trains for ease of assembly, or clearance fit is employed in each mating surface. The clearance of the reserved assembly and the clearance fit produce the axial runout. The addition of reserved clearance improves the accuracy of the transmission error estimate. As a consequence, the clearance-induced rotation angle error is given by:

$$\theta_a = \sqrt{\theta_{Jx}^2 + \theta_{Jy}^2} cos\gamma \tag{17}$$

where $\theta_{Jx}$ and $\theta_{Jy}$ are the clearance-induced rotation errors of the gear axis around the x- and y-axes, respectively. $\theta_{Jx} = \frac{\Delta_J}{R}$ and $\theta_{Jy} = \frac{\Delta_J}{R}$ may be used to calculate $\theta_{Jx}$ and $\theta_{Jy}$. The dividing circle radius of the gear is $R$, and the maximum clearance value or clearance after assembly adjustment required by design is $\Delta_J$. The phase angle of eccentric assembly, $\gamma$, is a uniform distribution in the range of $[0, 2\pi]$.

#### 4) TOOTH PITCH ERRORS

The common error factors contribute to tooth pitch mistakes: the tangential error of the dividing circle, as well as changes in tooth pitch due to gear runout and tooth profile form failures. It indicates the angle variation error of the gear in turning a pitch angle ($360^0/z$), which might damage the gear transmission's stability, and its value is $-f_{pt} \leq \Delta f_{pt} \leq f_{pt}$. The tooth pitch's linear error is converted to an angular error on the gear dividing circle, and Monte Carlo is used to simulate the error fluctuation on each tooth pitch of the gear. As a result, the tooth pitch error's angular error $\Delta p_k$ may be determined. Consequently, the angular error $\Delta p_k$ due to the tooth pitch error can be calculated as follows:

$$\Delta p_k = \frac{\Delta f_{pt}}{1000R} \times \frac{180}{\pi} \times 60 = \frac{10.8\Delta f_{pt}}{\pi R} \tag{18}$$

where $f_{pt}(\mu m)$ represents the limit deviation of individual tooth pitch; $R = mz/2(mm)$ is the theoretical dividing circle radius of the gear, $m$ refers to the module ($mm$), and $z$ is the number of teeth. In general, the accuracy of the rig's raising and lowering actions is determined by the geometry of the gear and rack system. When the teeth are geometrically defective, the gear and rack system's performance suffers. However, defects in gear and rack transmission systems include radial misalignment, axial misalignment, tooth profile misalignment, pitch, and other unexplained flaws, among others. The major source of the system's model error is this factor. Uncertainty factors induced by this parameter enhance control complexity while simultaneously promoting the system's self-adaptability. This inaccuracy is treated as a random effect during simulation and experimentation as part of the suggested approach toward a robust adaptive for the mechanical system.

*Assumption 3:* On the gear dividing circle, the linear error of the tooth pitch is bound and converted to an angular error.

*Assumption 4:* Assume that a maximum value of the error for control and normally states is comprehended or may be determined for each state.

*Remark 2* The error fluctuation on each tooth pitch of the gear is simulated using Monte Carlo, which utilizes a normal distribution (a normal distribution indicates that outcomes are evenly distributed around the mean). The position error bound is a basic limit of position accuracy for ultrawide bandwidth systems working in allowed conditions.

## IV. PARTICLE SWARM OPTIMIZATION SELF-ADAPTIVE FUZZY CONTROL APPROACH

### A. FUZZY CONTROLLER

In this study, the authors apply a fuzzy model including a double-input signal $e, de/dt$, and a single-output signal $u$ [18]. The fuzzy model consists of a set of rules and their consequences, which are often assumed to be linear functions of the inputs. If-Then rules are represented as a rule notation form within $B^i$ as follows:

$$R_i:\ If\ \chi_1\ is\ L_1^i \ldots and\ \chi_n\ is\ L_n^i then\ u\ is\ B^i \tag{19}$$

where ${L_1}^i, {L_2}^i, ..{L_n}^i \in R^h$ and $B^i \in R^h$ are indicates the fuzzy sets of output signal and input signals [38]. By using the singleton fuzzifier, the Max-Prod inference rule and the center averaged defuzzifier, the output signal $u$ is defined as

$$u(\chi) = \frac{\sum_{i=1}^{m} B^i[\prod_{j=1}^{n} \mu_{L_j^i}(\chi_j)]}{\sum_{i=1}^{m} [\prod_{j=1}^{n} \mu_{L_j^i}(\chi_j)]} \tag{20}$$

for $m$ is the amount of fuzzy rules, $\mu_{L_j^i}(\chi_j)$ indicates the Membership Functions (MFs). We get

$$\delta^T = [\bar{\delta}^1, \bar{\delta}^2, \ldots, \bar{\delta}^m]^T \in R^m \tag{21}$$

as the fuzzy parameter vector. Define the fuzzy basis functions with $\phi$ is represented as follows:

$$\phi_i(\chi) = \frac{[\prod_{j=1}^{n} \mu_{L_j^i}(\chi_j)]}{\sum_{i=1}^{h} [\prod_{j=1}^{n} \mu_{L_j^i}(\chi_j)]} \tag{22}$$

and define $\phi(\chi) = [\phi_1(\chi), \phi_2(\chi), \ldots, \phi_m(\chi)]^T$ as the fuzzy basis function vector. Thus, the fuzzy output is able to be

expressed as the linearization parametric form

$$u(\chi) = \delta^T \phi(\chi) \tag{23}$$

*Lemma 1 [39]:* For any given real continuous function $\varphi(\chi)$ on the compact set $\Omega \subset R^n$ and arbitrary $\xi > 0$, there exists a fuzzy system $u(\chi)$ in the form of an equation as

$$sup_{\chi \in \Omega} |\varphi(\chi) - \delta^T \phi(\chi)| \leq \xi \tag{24}$$

According to *Lemma 1*, the nonlinear function $\varphi(\chi)$ can be approximated as

$$\varphi(\chi, \delta) = \delta^T \phi(\chi) \tag{25}$$

Thus

$$\delta^* = argmin_{\delta \in \Omega}[sup_{x \in Z} |\varphi(\chi) - \varphi(\chi, \delta^*)|] \tag{26}$$

therein, $Z$ and $\Omega$, respectively, are compact regions for $\chi$ and $\delta$. Hence, define the minimum approximation error as

$$\xi = \varphi(\chi) - \delta^{*T} \phi(\chi) \tag{27}$$

### B. ADAPTIVE FUZZY CONTROLLER

We establish a AFC structure on m.file format with the MFs flexible value to improve the structure of controller. Therefore, the fuzzy modulator has a single-output $u_P(\chi)$ and a double-input $e(t)$, $de/dt$. The fuzzy output performance is represented as

$$u_P(\chi) = \frac{\sum_{i=1}^{m} B^i [\prod_{j=1}^{n} \mu_{L_{\lambda j}^i}(\chi_j)]}{\sum_{i=1}^{m} [\prod_{j=1}^{n} \mu_{L_{\lambda j}^i}(\chi_j)]} \tag{28}$$

therein, $\mu_{A_1^j}(\chi_1) = [\lambda_1(L_1^1, L_1^2, \ldots L_1^j)]$ is the fuzzy set of the error $e(t)$, $\mu_{A_2^j}(\chi_2) = [\lambda_2(L_2^1, L_2^2, \ldots L_2^j)]$ is the fuzzy set of the error-velocity $de/dt$, and $B_\lambda^i = [(\lambda_3 + \lambda_4/s)(B^1, B^2, \ldots B^i)]$ is the fuzzy set of output $u_p(\chi)$. The fuzzy inference $i$ is represented by the $j$ coefficient, which is an index of the fuzzy set. Then, $\phi_\lambda(\chi) = [\phi_\lambda^1, \phi_\lambda^2, \ldots, \phi_\lambda^m] \in R^m$ expresses the fuzzy basic vector which is determined as

$$\phi_\lambda(\chi) = \frac{[\prod_{j=1}^{n} \mu_{L_{\lambda j}^i}(\chi)]}{\sum_{i=1}^{m} [\prod_{j=1}^{n} \mu_{L_{\lambda j}^i}(\chi)]} \tag{29}$$

Following eq. (28), the AFC response can be described as

$$u_P(\chi) = \delta_\lambda^T \phi_\lambda(\chi) \tag{30}$$

### C. PROPOSED PSO-SELF ADAPTIVE FUZZY CONTROLLER

We apply the PSO algorithm to calibrate the parameter of MFs because it's easily implemented and computationally efficient. In this study, the PSO algorithm is used to find the optimal parameter controllers for operating the JuR nonlinear object in conditions of Assumptions 1, 2, 3, and 4. The determination of optimal coefficient $\lambda_i$ based on PSO algorithm [40], to deal with the improving control quality in the time-varying environment is represented in Algorithm 1. The PSO algorithm completes the correction of fuzzy set values with coefficient $\lambda_i$ to achieve the optimal parameters. Where, $y_d$ is the desired position, $y$ is the JuR response, $u_P(\chi)$ is the input control to JuR model, $\beta$ is a constant and $\epsilon$ is a small constant. The second term of eq. (36) is to obtain the minimum input control $u_P(\chi)$, and controlled by $\beta$.

**Algorithm 1** The PSO algorithm calibrates the MFs values [21]

Initialization: **for each** particle $i(1 \leq i \leq s)$ **do**
Randomly initialize the position $\lambda_i^p(k)$
Randomly initialize the velocity $v_i(k)$
Initialize calibration coefficient $\lambda_i(\lambda_1, \lambda_2, \lambda_3, \lambda_4)$
**end for**
**for each** iteration $k$ **do**
(a) Each particle $\lambda_i^p(k)$ update the values of $\lambda_{i,j}^p(k)$ and $\lambda_{i,j}^{Gb}(k)$

$$\lambda_{i,j}^p(k+1) = \begin{cases} \lambda_{i,j}^p(k), \; if \; J(\lambda_{i,j}^p(k+1)) \geq J(\lambda_{i,j}^p(k)) \\ \lambda_{i,j}^p(k+1), \qquad otherwise \end{cases} \tag{31}$$

$$\lambda_{i,j}^{Gb}(k+1) = argmin_{\lambda_{i,j}^{Pb}} J(\lambda_{i,j}^{Pb}(k+1)), 1 \leq i \leq s \tag{32}$$

(b) Initialize the particle attribute $v_i(k)$

$$\begin{aligned} v_{i,j}(k+1) = \; & w(k) v_{i,j}(k) + c_1 r_1 [\lambda_{i,j}^{pb}(k) - \lambda_{i,j}^p(k)] \\ & + c_2 r_2 [\lambda_j^{Gb}(k) - \lambda_{i,j}^p(k)] \end{aligned} \tag{33}$$

where

$$w(g) = \frac{(iter_{max} - g)(w_{max} - w_{min})}{iter_{max}} + w_{min} \tag{34}$$

(c) Determine the new position $\lambda_{i,j}^p(k)$

$$\lambda_{i,j}^p(k+1) = \lambda_{i,j}^p(k) + v_{i,j}(k+1) \tag{35}$$

(d) Apply newly coefficient $\lambda_{i,j}^p(k)$ to adjust the amplitude values of the MFs and compute a fitness value according to the criteria efficiency.

$$\sum_{t=0}^{t_f} ||y - y_d|| + \beta \sum_{t=0}^{t_f} ||u_P(\chi)|| < \epsilon \tag{36}$$

(e) A suitable point to start is to compare the obtained value to the termination condition. If the convergence criteria do not fulfill the criterion, raise k and return to step 1. (a).
**end for**

The search process of the values $\lambda_i(\lambda_1, \lambda_2, \lambda_3, \lambda_4)$ carries out in 4-dimensional space. The limited search range will lead to locally convergent values (express at Definition 1). A large search space will achieve a globally optimal solution (such as Definition 2), but the convergence time will be slow. Definitions 1 and 2 are defined as follows:

*Definition 1 [41]:* Local convergence $\hat{\lambda} \in D$ of a fitness function $f: D \leftarrow \Re$ is the input element with $f(\hat{\lambda}) > f(\lambda)$ for $\forall\lambda$ in the surroundings of $\hat{\lambda}$. Define

$$\hat{\lambda} : \exists \epsilon > 0 : f(\hat{\lambda}) > f(\lambda) \forall \lambda \in D, |\lambda - \hat{\lambda}| < \epsilon \tag{37}$$

*Definition 2 [41]:* Global convergence $\lambda^* \in D$ of a fitness function $f: D \leftarrow \Re$ is the input element with $f(\lambda^*) > f(\lambda)$ for $\forall\lambda$. We get

$$\lambda^* : f(\lambda^*) > f(\lambda) \forall \in D \tag{38}$$

The fuzzy control gives different results for nonlinear systems like the JuR model. So if we choose the Lyapunov function $\dot{V}(\chi)$ only has a *Negative* value, and the approximate of the nonlinear components are not satisfied. Thus, our method is to combine the parameters of the adaptation and the fuzzy controller so that the PSO searching obtains the negative derivative of Lyapunov function $\dot{V}_{de}(\chi)$ [41], that is

$$\dot{V}_{de}(\chi) \leq -\sigma V(\chi) \tag{39}$$

where $\sigma > 0$, that will give an exponential convergence rate. The new performance index criteria can be rewritten by

$$\sum_{t=0}^{t_f} ||y - y_d|| + \beta \sum_{t=0}^{t_f} \xi_v < \epsilon \tag{40}$$

therein, $\xi_v$ represents the erroneous of the desired derivative Lyapunov function, which is defined as

$$\xi_v(\chi) = \begin{cases} 0 & \dot{V}(\chi) \leq \dot{V}_{de}(\chi) \\ ||\dot{V}(\chi) - \dot{V}_{de}(\chi)|| & \dot{V}(\chi) > \dot{V}_{de}(\chi) \end{cases} \tag{41}$$

The goal of the PSO-SAFC solution is to bring $\xi_v$ to zero, that is, $\dot{V}(\chi) \leq \dot{V}_{de}(\chi)$. Minimum the erroneous of the desired derivative Lyapunov function $\xi_v$ depends on the SAFC coefficient $\delta_\lambda^T$ (express at Eq. (27)) under working conditions in Remarks 1, 2, and Assumption 2. So the approximation error $\xi_v$ is always initial within the limit range [32], satisfy

$$\lim_{t\to\infty} ||\xi_v|| = \lim_{t\to\infty} ||\varphi(\chi) - \delta_\lambda^{*T}\phi(\chi)|| = 0 \tag{42}$$

Based on the stable condition (at Eq. (39)), $\dot{V}_{de}(\chi)$ is less than $-\sigma V(\chi)$, so $\dot{V}(\chi)$ can be converted as follows [41]

$$\dot{V}(\chi) \approx \Delta V(\chi) = \frac{V_j(\chi) - V_{j-1}(\chi)}{\Delta t} \tag{43}$$

The PSO-SAFC solution ensures self-adaptive by $\delta_\lambda^{*T}$ coefficient within a limited range (Eq. (42)), and process control under stable conditions (Eq. (39)) through the Lyapunov evaluation constraint (Eq. (27)). Thereby, the proposed PSO-SAFC guarantees that the JuR closed-loop control system is stable and enables tracking of the control goal.

## V. EVALUATION STUDIES

### A. ANALYSIS OF PROPOSED CONTROL APPROACH BY SIMULATION STUDIES

#### 1) CONFIGURATION PARAMETER

Table 4 presents the parameter dimensions of the TamDao05 JuR model which is scaled down by the ratio of 1:100. The parameters of the environmental impact are given in the Table 5. The purpose of this work is to use simulation and experimental contents to make it easier to design, build, and operate embedded systems using Matlab. We begin by constructing the JuR legs, which will be powered by DC motor pluses through the shaft system as in Eqs (6) to (10). We used the Matlab 2019b software to simulate the JuR model under the same climatic conditions and with the same parameters.

**TABLE 4. Parameter of JuR model dimensions [21].**

| DESCRIPTION | SYMBOL | SPECIFICATIONS |
|---|---|---|
| Length overall | $H$ | 1.62 $m$ |
| Breadth overall | $B$ | 0.96 $m$ |
| Hull height | $h$ | 0.232 $m$ |
| Hullweight | $M_{hull}$ | 0.0327 $ton$ |
| Weight of a leg of the rig | $M_{leg}$ | 0.012 $ton$ |
| Jack-up weight | $M_{JuR}$ | 0.0928 $ton$ |
| Number of DC motor | | 06 |
| Conversion factor | $k_e$ | 33.33 |
| Torque constant | $K_t$ | 1.28 |
| Armature resistance | $R_a$ | 11.4 |
| Back emf constant | $K_b$ | 0.0045 |
| Inductance | $L_a$ | 0.1214 |
| Rotor inertia | $J$ | 0.02215 |
| Viscous friction constant | $D_a$ | 0.002953 |

**TABLE 5. The environmental parameters [21].**

| DESCRIPTION | SYMBOL | SPECIFICATIONS |
|---|---|---|
| Wave height | $H_s$ | 0.8 $m$ |
| Wave spectrum peak frequency | $\omega_0$ | 0 $rad/s$ |
| Wave direction | $\psi_0$ | $30^o$ |
| Spreading factor | $s$ | 2 |
| Number of frequencies | $N$ | 20 |
| Number of directions | $M$ | 10 |
| Cutoff frequency factor | $\xi$ | 3 |
| Wave component energy limit | $k$ | 0.005 |
| Wave direction limit | $\psi_{lim}$ | 0 |
| Wind traction into the ichnography region | $A_T$ | 2.4 |
| Wind speed | $V_\omega$ | 2 $m/s$ |
| Angle of impact wind | $\beta_\omega$ | $20^o$ |
| Current speed | $V_c$ | 2 $m/s$ |
| Jack-up direction | $\beta_c$ | $30^o$ |
| Low frequency and high frequency of rotation | $\psi_L, \psi_H$ | $0^o$ |
| Dominating wave frequency | $\omega_0$ | 0.8976 $rad/s$ |
| Damping coefficient | $\lambda$ | 0.1 |
| Wave intensity | $\sigma$ | $\sqrt{2}$ |

The fuzzy's structure is based on the m.file matlab code, which helps the PSO searching algorithm easier to identify the convergence value. These optimal coefficients aim to adjust the MFs value of the fuzzy controller to fulfill the control requirement.

#### 2) FUZZY-PID CONTROLLER DESIGN

In this subsection, the authors will compare the JuR positioning response of the proposed PSO-SAFC controller in this paper with that of the FPID controller as follows:

$$u_{FPID}(s) = K_p(s)e(s) + K_i(s)\int_0^s e(s)ds + K_d(s)\frac{de}{ds} \tag{44}$$

The coefficients $K_p(s)$, $K_i(s)$, and $K_d(s)$ have a flexible structure according to the input variable error instead of the fixed coefficients $K_p = diag(5.004 \times 10^{-3}, 6.014 \times 10^{-3}, 5.315 \times 10^{-3})$, $K_i = diag(2.381 \times 10^{-5}, 1.973 \times 10^{-5}, 2.537 \times 10^{-5})$, $K_d = diag(14.39 \times 10^{-3}, 12.74 \times 10^{-3}, 16.02 \times 10^{-3})$, respectively. The flexible coefficients $K_p(s)$, $K_i(s)$, and $K_d(s)$ are updated after each

**TABLE 6. Parameter setting of PSO-SAFC.**

| DESCRIPTION | SYMBOL | SPECIFICATIONS |
|---|---|---|
| Generation number | $k$ | 20 |
| Population size | $iter$ | 60 |
| Search space | $n$ | 4 |
| Upper bound | $ub$ | $2 \times 10^{18}$ |
| Lower bound | $lb$ | 1 |
| Maximum inertia weight | $w_{max}$ | 0.9 |
| Minimum inertia weight | $w_{min}$ | 0.1 |
| Acceleration coefficient of the individual | $c_1$ | 0.01 |
| Acceleration coefficient of the population | $c_2$ | 1 |
| Best convergence | | $8.97409 \times 10^{-4}$ |

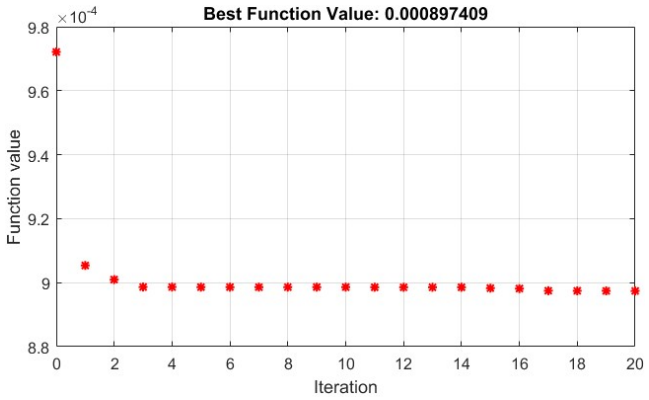


**FIGURE 3. Convergence performance of PSO-SAFC.**

control cycle according to the erroneous amplitude. The Proportional Integral Derivative (PID) coefficient is updated by:

$$\begin{cases} K_p(s) = K_p(s-1) + u_f(\Delta k_p) \\ K_i(s) = K_i(s-1) + u_f(\Delta k_i) \\ K_d(s) = K_d(s-1) + u_f(\Delta k_d) \end{cases} \quad (45)$$

The updated coefficients $u_f\left(u_f(\Delta k_p), u_f(\Delta k_i), u_f(\Delta k_d)\right)$ are defined by fuzzy system. The notation of MFs for *NB* is Large Negative, for *NBB* is Near Big Negative, for *NS* is Small Negative, for *NSS* is Near Small Negative, for *ZE* is Zero, for *PSS* is Near Small Positive, for *PS* is Small Positive, for *PBB* is Near Big Positive, and for *PB* is Large Positive. We use a fuzzy system with a double-input $e(t) = [-0.5 \div 0.5]$, $de/d(t) = [-10 \div 10]$, and a triple-output $\Delta k_p = [60 \div 100]$, $\Delta k_i = [0 \div 1]$, and $\Delta k_d = [0 \div 50]$ to calibrate the coefficients $K_p(s)$, $K_i(s)$, and $K_d(s)$ [21].

### 3) PSO-SAFC CONTROLLER DESIGN

To fairly compare the simulation results obtained, PSO-SAFC and other solutions apply the same number of training parameters and vessel structure modelling. The performance of PSO-SAFC is compared with that of the FPID [35] for JS control. In this study, we use the PSO searching parameters as same as Table 6 for implementing the proposed system. Then, the searching process of $\lambda_i$ optimal coefficient is randomly generated. Thus, 20 iteration were applied with random initial models so that every iteration process could be able to wear a

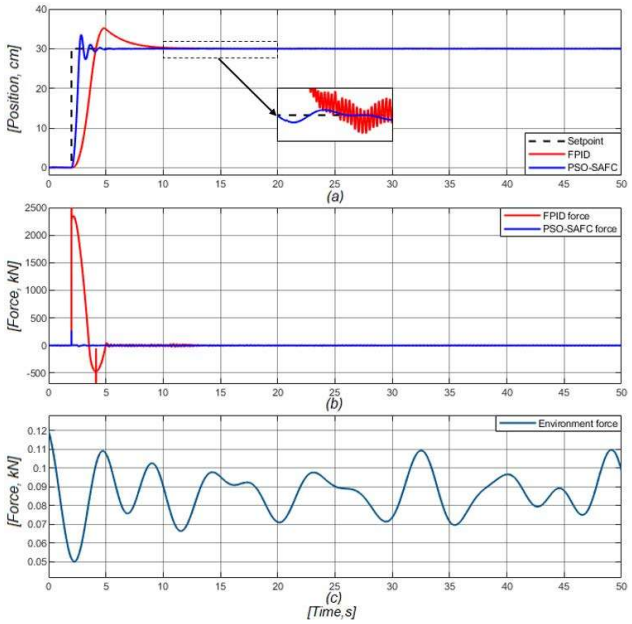


**FIGURE 4. The performance of case study 1 includes both controllers. (a) Actual position of JuR system. (b) FPID control force and PSO-SAFC control force. (c) Total forces from environment.**

**TABLE 7. A comparison of the effectiveness of several solutions for Case Study 1.**

| Solution | Membership functions | Response time | Overshoot | Fluctuation |
|---|---|---|---|---|
| Fuzzy [42] | 69 | 7.0s | 6.5cm | 0.050cm |
| FPID [21] | 69 | 6.5s | 5.5cm | 0.035cm |
| AFC [19] | 69 | 4.5s | 5.0cm | 0.045cm |
| PSO-SAFC | 69 | 2.5s | 3.5cm | 0.020cm |

different position to search the JuR control. Through searching process, the best convergence result is $8.97409 \times 10^{-4}$ which corresponds to $\lambda_i$ ($\lambda_1$, $\lambda_2$, $\lambda_3$, $\lambda_4$) values. In addition, the convergence performance of PSO-SAFC is described in detail by Fig. 3. The best fitness value and the mean fitness value are getting closer and obtaining better performance.

### 4) NUMERICAL SIMULATIONS

Comparison of simulation results obtained when using FPID and PSO-SAFC controllers are presented as shown in Fig. 4, and Fig. 5. Figures 4(a), and Fig. 5(a) show the actual position response of the JuR under the impact of environmental forces when applying the FPID approach (red line) and the PSO-SAFC approach (blue line). Figures 4(b), and Fig. 5(b) are the results obtained when the force is applied. Besides that, Fig. 4(c), and Fig. 5(c) express the environmental force acting on the truss. The environmental forces $\tau_d$, act on the kinetic model of JuR (expressed by eq.(1)) and the thrusters dynamic $\tau_i$, cause the JuR response erroneous. The PSO-SAFC approach (presented in section III) is conducted on TamDao05 JuR model in two cases study.

*Case study 1:* The simulation results that apply the FPID and PSO-SAFC controllers are pointed out in Fig. 4 with the

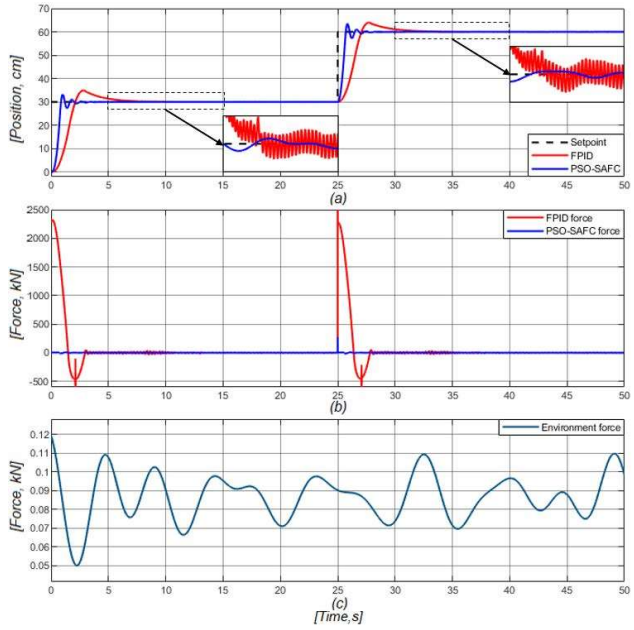


**FIGURE 5.** The performance of case study 2 includes both controllers. (a) Actual position of the JuR system. (b) FPID control force and PSO-SAFC control force. (c) Total forces from environment.

**TABLE 8.** A comparison of the effectiveness of several solutions for Case Study 2.

| Solution | Membership functions | Response time | Overshoot | Fluctuation |
|---|---|---|---|---|
| Fuzzy [42] | 69 | 6.5s | 7.0cm | 0.055cm |
| FPID [21] | 69 | 5.5s | 5.5cm | 0.050cm |
| AFC [19] | 69 | 4.0s | 4.5cm | 0.050cm |
| PSO-SAFC | 69 | 3.0s | 3.0cm | 0.035cm |

**TABLE 9.** Parameter of the UT-JuR 01 model dimensions.

| DESCRIPTION | SYMBOL | SPECIFICATIONS |
|---|---|---|
| Engine power | $P$ | 60 $W$ |
| Load speed | $N$ | 468 $rpm$ |
| Rated load torque | $T$ | 15 $kgf/cm$ |
| Ratio of motor | $u$ | 19.2:1 |
| Rated current | $I$ | 6.5 $A$ |
| Module of gear | $m$ | 1.5 $mm$ |
| Pressure angle of basic | $\alpha$ | $20^0$ |
| Diameter of gear | $D$ | 30 $mm$ |
| Pitch of gear | $p$ | 4.71 $mm$ |
| Face width | $b$ | 10 $mm$ |
| Length rack | $l$ | 1600 $mm$ |
| Central processing control | $STM32F749NG$ | 01 |
| Inclination angle sensor | $MPU6050$ | $Yaw, Pitch, Roll$ |
| Position sensor | $Encoder$ | $LegsA, B, C$ |
| DC control driver | $PWM$ | $06DCmotors$ |

optimal coefficient $\lambda_i(1.279 \times 10^{18}, 1.828 \times 10^{18}, 1.225 \times 10^{18}, 8.734 \times 10^{17})$ and the limitations of adaptive coefficient $\delta_{min}(-1.7053 \times 10^{17}) \leq \delta_i \leq \delta_{max}(1.7053 \times 10^{17})$. The JuR model moved to the desired position (30 cm) by using the FPID and PSO-SAFC controllers under the influence of the environment in around 48 seconds. The overshoot, response time, and fluctuation criteria are all satisfied by the proposed result of the JuR location shown in Fig. 4(a). Table 7 presents the findings of the comparisons made between the suggested method and those of Fuzzy controller [42] and FPID controller [21], and Adaptive Fuzzy Controller (AFC) [19]. Maximum overshoot, PSO-SAFC, AFC, FPID, and Fuzzy values are 3.5 cm, 5 cm, 5.5 cm, and 6.5 cm, respectively, in the details. The Fuzzy, FPID, and AFC all have reaction times that are slower than the proposed PSO-SAFC, which has a response time of about 4.5 seconds, 4 seconds, and 2 seconds. The proposed solution with the self-adaptive coefficient $\delta_i$ has reduced the amplitude of fluctuations and overshoots caused by the impact of the environment, thereby making the JuR response in a low erroneous case. Besides, the optimal correction coefficient $\lambda_i$ helps the proposed solution to provide a better response than the others. Additionally, PSO-SAFC has a substantially smaller fluctuation amplitude than the competition.

*Case study 2:* The JuR model moved to the desired position (30 cm) by using the FPID and PSO-SAFC controllers under the influence of the environment in this example, the rig body is moved to the predetermined position (30 cm) while counteracting external forces, and then they keep lifting it until it reaches 60 cm from the 30 cm reference position at the 25th-second. In the first scenario, the identical PSO-SAFC controller parameters are utilized. According to Fig. 5(a), the PSO-SAFC controller has a roughly smaller overshoot amplitude than the FPID controller. Therefore, the comparison findings in Table 8 demonstrate that the overshoot of PSO-SAFC is around 4 cm, 2.5 cm, and 1.5 cm less than those of the Fuzzy, the FPID, and the AFC. The fluctuation value using the PSO-SAFC is lower than the 0.015 cm value using the AFC. Changing the reference position in combination with environmental influences will make the JuR position erroneously higher than case 1. The results using the PSO-SAFC solution still maintain the JuR position in the stable domain with self-correction coefficient $\delta_i$ and guarantee the response quality with the optimal coefficient $\lambda_i$. The comparative findings therefore show that the PSO-SAFC solution meets the technical criteria in a good manner. It is clear that the proposed PSO-SAFC controller can keep the JuR response quality stable even when the set-point conditions change.

### *B. ANALYSIS OF PROPOSED CONTROL APPROACH BY EXPERIMENT STUDIES*

In this study, with parameter of JuR model dimensions in Table 4, the main parameters of the UT-JuR 01 are presented in Table 9

To control the DC motor system for lifting the JuR, the authors use Matlab software to implement the proposed real-time PSO-SAFC and real-time FPID controllers into the main processor STM32F746NG. Six DC motors are used to move the JS up and down on three movable legs and to the required position. Therefore, the computer receives the experimental model's response signal through the UART standard and syn-

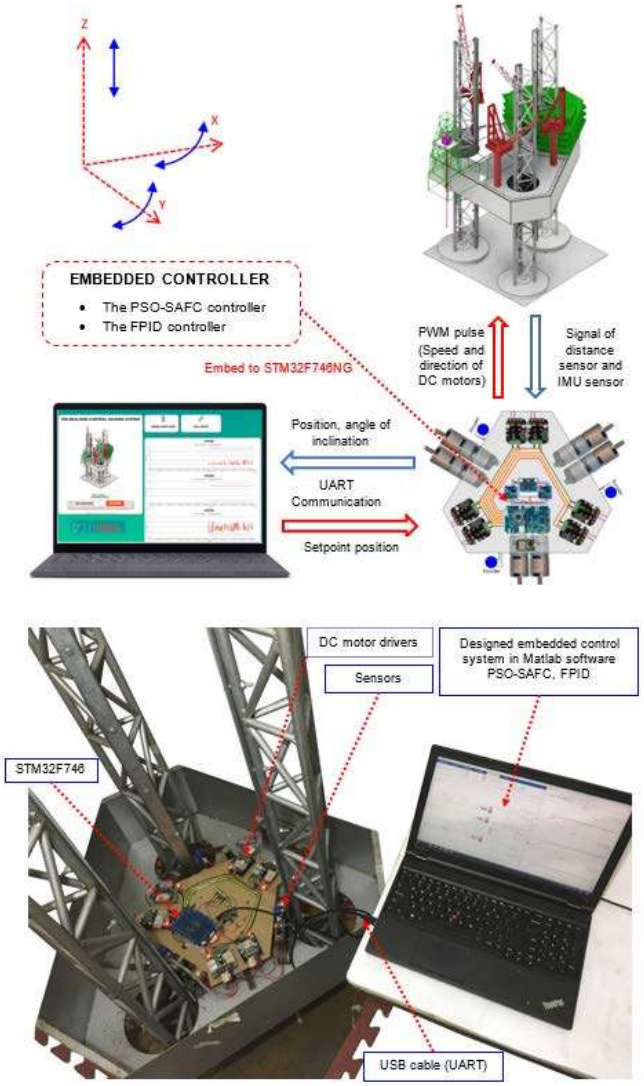


**FIGURE 6.** Overall structure of JuR experiment model.

thesizes it into charts for analysis. Last but not least, Fig. 6 depicts the JuR experiment model (named UT-JuR 01). The following is the operating principle:

- The distance sensors (Encoder) locate the JuR body, and the IMU sensor block detects the JuR's inclination. The feedback signal is then sent to the STM32F746NG central processor via the ADC converter circuit.
- To determine the value of the control signal, the real-time embedded controller compares the values of the desired signal and the feedback signal.
- To raise and lower the JuR to the necessary position, the driver circuit converts the control signal into a PWM pulse that controls the speed and direction of the DC motor.

The experiment study is conducted in two examples in this section to verify the efficacy and adaptability of the proposed PSO-SAFC approach against changing environmental conditions. Figures 8 and 9 depict the JuR's actual 3-leg reaction while using the FPID embedded technique (red line) and the PSO-SAFC embedded approach, respectively, during the lifting of the rig body (blue line).

### 1) EXPERIMENT STUDIES IN UT-JuR 01

#### *a: EXPERIMENT CASE STUDY 1*

In this scenario, the real-time embedded controllers for the FPID and PSO-SAFC force the JuR's experiment model to the desired position of 30 cm from the reference position of 00 cm and keep it balanced for 580 seconds (Fig. 8). Moreover, adopting the PSO-SAFC approach as opposed to the FPID at 1.35 cm, the Rig legs' oscillation amplitude is less. Additionally, the proposed PSO-SAFC solution and the FPID solution have reaction times of 120 and 135 seconds, respectively. Consequently, the suggested solution is precise, extremely effective in the actual process, and satisfies the quality standards.

Then real-time embedded controllers continue to lift the experiment model to position 60 cm from the reference of 30 cm at the 300th-second.

#### *b: EXPERIMENT CASE STUDY 2*

In this case, the real-time embedded controllers for the FPID and PSO-SAFC force the JuR model to the designated point (30 cm) in approximately 280 seconds. The experiment model is then raised by embedded controls until it is 60 cm from the set point of 30 cm at the 300th-second. Figure 9 displays the outcomes of experimental case 2. The reaction time for the PSO-SAFC scenario is 120 seconds, which is quicker than the FPID solution's 155 seconds response time. The response amplitude that implements the suggested PSO-SAFC solution changes gradually over time rather than all at once. When utilizing the PSO-SAFC controller, the JuR legs' oscillation amplitude is 1.55 cm less than comparing with the FPID controller. Thus, it has been demonstrated that the proposed control approach works well under real-world circumstances. To adequately illustrate the proposed approach, the JuR experimental model has to be tested extensively in various working modes, extensively in various working modes.

### 2) EVALUATE SOME EXPERIMENTAL RESULTS

Following is a summary of the key aspects based on analysis of two experimental cases, as shown in Figures 8 and 9.

- Although the PSO-SAFC response is more consistent than FPID, the results are not significantly different because of the high sensor noise, the identical mechanical components on the hardware, and the reaction delay of an actuator.
- When both controllers are based on fuzzy technology, they maintain the feature of fuzzy sets, which is sharp impulse responses (because the membership function is a built-in isosceles triangle. This response characteristic can be improved when the number of fuzzy laws increases. As there are more fuzzy regulations, this response characteristic can be enhanced. In this study, we only employed 23 membership functions integrating

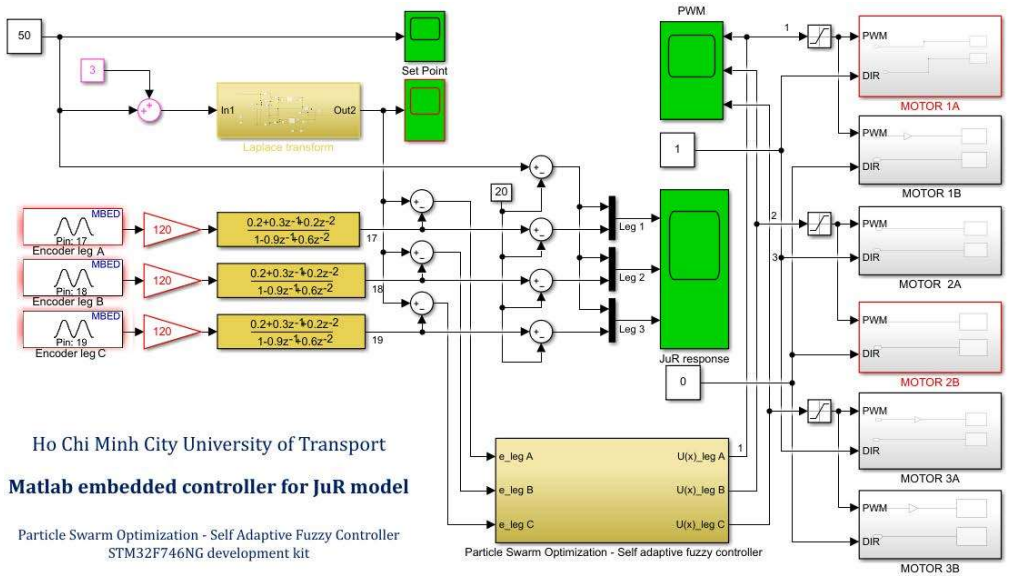


**FIGURE 7.** Embedded PSO-SAFC controller for UT-JuR 01.

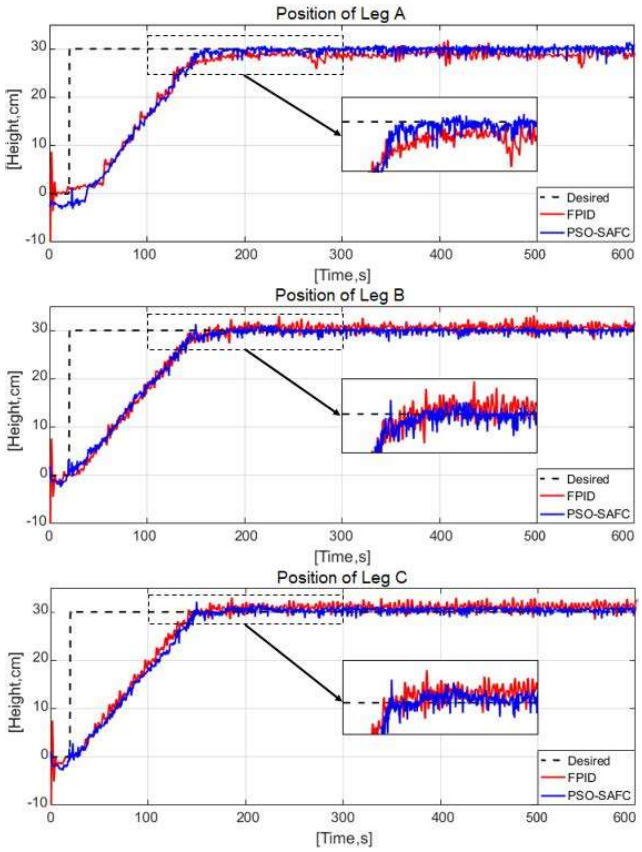


**FIGURE 8.** The experimental result using the FPID embedded controller in case 1.

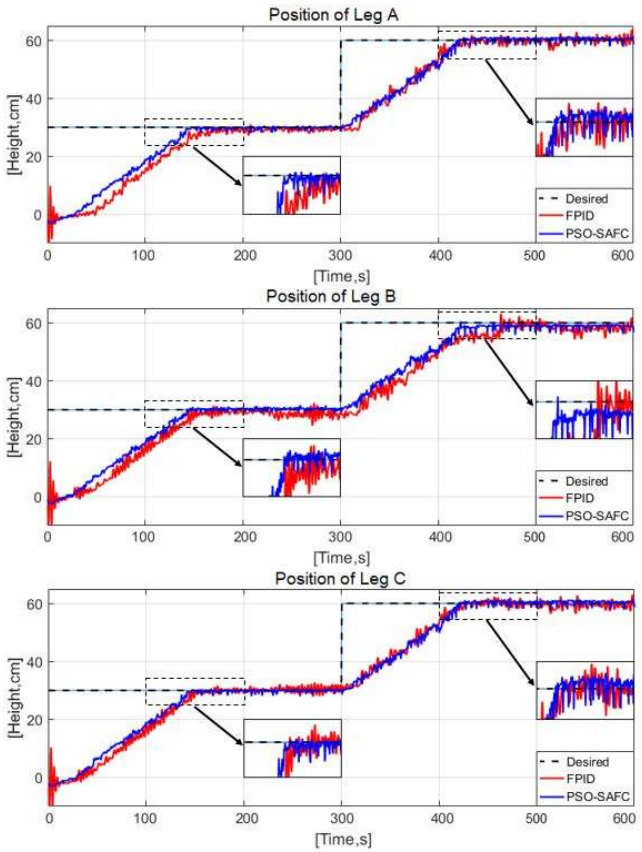


**FIGURE 9.** The experimental result using the FPID embedded controller in case 2.

35 rules for each JuR leg controller due to the slow processing speed of the central controller.

- The PSO-SAFC controller's position response on three JuR legs is more even than the FPID's. Although there is some deviation, the overshoot amplitude remains within the permitted range. The realistic outcomes demonstrate that PSO-SAFC is superior to other approache.

In light of the additional experimental findings listed in Table 10, which were deemed satisfactory, we proceed with the relevant observations:

**TABLE 10. Control test results at the model.**

| Experiment | Leg A | Leg B | Leg C | Center of JuR | Request to be achieved |
|---|---|---|---|---|---|
| Position 0 to 300(mm) | 286.5 | 293.5 | 291.5 | 290.5 | 300±6% |
| Response time | 3.5s | 4.0s | 4.0s | 4.0s | 5.5s |
| Position deviation between legs | | | 531.5 | | 520±5% |
| Position 300 to 600(mm) | 587.5 | 590.5 | 589.0 | 589.5 | 600±6% |
| Response time | 4.5s | 4.0s | 4.5s | 4.5s | 5.5s |
| Position deviation between legs | | | 536.5 | | 520±5% |
| Position 300 to 800(mm) | 782.5 | 786.5 | 785.5 | 784.5 | 800±6% |
| Response time | 5.0s | 5.0s | 4.5s | 5.0s | 5.5s |
| Position deviation between legs | | | 540.8 | | 520±5% |

- In all 3 experiment cases in Table 10, the legs position oscillation amplitudes yielded with the established quality of the achieved request(< 6%).
- The are no hard fluctuations within the response amplitude changes steadily over time.
- In experimental conditions, the shortest reaction time needed to attain the equilibrium value is within the permitted range (< 5.5 seconds).

The experimental model of the JuR needs to be tested more in different working modes in order to effectively demonstrate the proposed solution.

## VI. CONCLUSION

During sea state disturbances, the system is used automatically to regulate and stabilize the position of the JuR to prevent platforms from being shifted. In this paper, establishing a better control theory for a Jack-up Rig's jacking system is crucial.First, we use a PSO technique based on a fuzzy controller to examine how to adapt to the impacts of external forces, mechanical errors and hydrodynamic amplification. The Self Adaptive Fuzzy Particle Swarm Optimization controller is then compared to a Fuzzy Proportional Integral Derivative controller that meets Lyapunov requirements. By simulation on Matlab, the optimal coefficients $\lambda_i(1.279 \times 10^{18}, 1.828 \times 10^{18}, 1.225 \times 10^{18}, 8.734 \times 10^{17})$ are selected from PSO process, the results of two case studies on Table 7 and Table 8 indicating and demonstrating the performance of the proposed method. Next, the control algorithm is embedded in the STM32F746VG central processor, which gathers data on leg locations and JuR body tilt and compares it to command values to move the rig body and provide control signals to the Motor drive. Finally, the experiment results indicate the benefits of the proposed PSO-SAFC controller.

## REFERENCES

[1] Q. S. Yin, J. Yang, G. X. Xu, R. J. Xie, M. Tyagi, L. L. Li, X. Zhou, N. D. Hu, G. Tong, C. Fu, and D. Pang, "Field experimental investigation of punch-through for different operational conditions during the jack-up rig spudcan penetration in sand overlying clay," *J. Petroleum Sci. Eng.*, vol. 195, pp. 1–21, Dec. 2020.

[2] N. Shabakhty, "Durable reliability of jack-up platforms: The impact of fatigue, fracture and effect of extreme environmental loads on the structural reliability," Ph.D. thesis, Dept. Civil Eng., Delft Univ. Technol., Delft, The Netherlands, 2004.

[3] H. Zhou, B. Yi, Y. X. Niu, B. N. Wei, S. Z. Du, H. Q. Zhao, J. C. Liu, and J. C. Wang, "Application of efficient TEP FE computation on accurate fabrication of cylindrical leg structure of jack-up rig," *Ocean Eng.*, vol. 196, pp. 1–11, Jan. 2020.

[4] P. Hu, Z. Xiao, C. Leo, and S. Liyanapathirana, "Advances in the prediction of spudcan punch-through in double-layered soils," *Mar. Struct.*, vol. 79, pp. 103038–103053, Sep. 2021.

[5] T. I. Bø, A. R. Dahl, T. A. Johansen, E. Mathiesen, M. R. Miyazaki, E. Pedersen, R. Skjetne, A. J. Sørensen, L. Thorat, and K. K. Yum, "Marine vessel and power plant system simulator," *IEEE Access*, vol. 3, pp. 2065–2079, 2015.

[6] Y. M. A. Welaya, A. Elhewy, and M. Hegazy, "Investigation of jack-up leg extension for deep water operations," *Int. J. Nav. Archit. Ocean Eng.*, vol. 7, no. 2, pp. 288–300, Mar. 2015.

[7] A. R. El-gamal, A. Essa, and A. Ismail, "Effect of tethers tension force on the behavior of triangular tension leg platform," *Amer. J. Civil Eng. Archit.*, vol. 2, no. 3, pp. 107–114, May 2014.

[8] B. K. Young, "Dynamic analysis of multiple-body floating platforms couple with mooring lines and risers," Ph.D. dissertation, Dept. Ocean Eng., Texas Univ., Austin, TX, USA, 2003.

[9] J. Sætrom, H. Selseng, A. MacDonald, T. Kjølseth, and O. Kolbjørnsen, "Consistent integration of drill-stem test data into reservoir models on a giant field offshore Norway," in *Proc. SPE Annu. Tech. Conf. Exhib.*, 2013, pp. 1–18.

[10] E. Camponogara, A. F. Teixeira, E. O. Hulse, T. L. Silva, S. Sunjerga, and L. K. Miyatake, "Integrated methodology for production optimization from multiple offshore reservoirs in the santos basin," *IEEE Trans. Autom. Sci. Eng.*, vol. 14, no. 2, pp. 669–680, Apr. 2017.

[11] B. Wang, X. Wang, X. Wang, C. Shao, P. D. Judge, and T. C. Green, "An analytical approach to evaluate the reliability of offshore wind power plants considering environmental impact," *IEEE Trans. Sustain. Energy*, vol. 9, no. 1, pp. 249–260, Jan. 2018.

[12] S. M. Samindi M. K. Samarakoon and R. M. C. Ratnayake, "Minimization of risk assessments variability in technology qualification processes," *J. Offshore Mech. Arctic Eng.*, vol. 139, no. 2, pp. 1–8, Apr. 2017.

[13] K. V. Wong, "Need for engineering solutions to problems associated with offshore oil and gas production," *J. Energy Resour. Technol.*, vol. 136, no. 3, pp. 1–3, Sep. 2014.

[14] K. Satterlee, S. Watson, and E. Danenberger, "New opportunities for offshore oil and gas platforms—Efficient, effective, and adaptable facilities for offshore research, monitoring, and technology testing," in *Proc. OCEANS MTS/IEEE Charleston*, 2018, pp. 1–5.

[15] K. Liu, G. Chen, and W. Shao, "An efficient modeling and optimization approach for pressure testing during reentry operation of deepwater drilling riser system," *IEEE Access*, vol. 8, pp. 74759–74770, 2020.

[16] J.-S. Shin and J.-O. Kim, "Optimal design for offshore wind farm considering inner grid layout and offshore substation location," *IEEE Trans. Power Syst.*, vol. 32, no. 3, pp. 2041–2048, May 2017.

[17] X.-K. Dang and T.-D. Tran, "Modeling techniques and control strategies for jack-up rig: A state of the art and challenges," *IEEE Access*, vol. 9, pp. 155763–155787, 2021.

[18] X.-K. Dang, V.-D. Do, and X.-P. Nguyen, "Robust adaptive fuzzy control using genetic algorithm for dynamic positioning system," *IEEE Access*, vol. 8, pp. 222077–222092, 2020.

[19] V. D. Do, X. K. Dang, and A. T. Le, "Fuzzy adaptive interactive algorithm for rig balancing optimization," in *Proc. Int. Conf. Recent Adv. Signal Process., Telecommun. Comput. (SigTelCom)*, Jan. 2017, pp. 143–148.

[20] C. H. Lin and Y. K. Wu, "Overview of frequency-control technologies for a VSC-HVDC-integrated wind farm," *IEEE Access*, vol. 9, pp. 112893–112921, 2021.

[21] T. D. Tran, V. D. Do, X. K. Dang, and B. L. Mai, "Improving the control performance of jacking system of jack-up rig using self-adaptive fuzzy controller based on particle swarm optimization," in *Industrial Networks and Intelligent Systems* (Lecture Notes of the Institute for Computer Sciences, Social Informatics and Telecommunications Engineering), vol. 444. Cham, Switzerland: Springer, 2022, pp. 184–200.

[22] H. Dong, S. Gao, B. Ning, T. Tang, Y. Li, and K. P. Valavanis, "Error-driven nonlinear feedback design for fuzzy adaptive dynamic surface control of nonlinear systems with prescribed tracking performance," *IEEE Trans. Syst., Man, Cybern. Syst.*, vol. 50, no. 3, pp. 1013–1023, Mar. 2020.

[23] M. Ma, K. Sun, T. Wang, and J. Qiu, "Adaptive fuzzy risk-sensitive control for stochastic strict-feedback nonlinear systems with unknown uncertainties," *IEEE Trans. Fuzzy Syst.*, vol. 29, no. 12, pp. 3794–3802, Dec. 2021.

[24] M. Orouskhani, D. Shi, and X. Cheng, "A fuzzy adaptive dynamic NSGA-II with fuzzy-based Borda ranking method and its application to multimedia data analysis," *IEEE Trans. Fuzzy Syst.*, vol. 29, no. 1, pp. 118–128, Jan. 2021.

[25] V. Giordano, D. Naso, and B. Turchiano, "Combining genetic algorithms and Lyapunov-based adaptation for online design of fuzzy controllers," *IEEE Trans. Syst., Man, Cybern., B*, vol. 36, no. 5, pp. 1118–1127, Oct. 2006.
[26] X. Su, C. L. P. Chen, and Z. Liu, "Adaptive fuzzy control for uncertain nonlinear systems subject to full state constraints and actuator faults," *Inf. Sci.*, vol. 581, pp. 553–566, Dec. 2021.
[27] T. G. Yang, N. Sun, and Y. C. Fang, "Adaptive fuzzy control for a class of MIMO underactuated systems with plant uncertainties and actuator deadzones: Design and experiments," *IEEE Trans. Cybern.*, vol. 52, no. 8, pp. 8213–8226, Aug. 2022.
[28] N. Priyadarshi, S. Padmanaban, J. B. Holm-Nielsen, F. Blaabjerg, and M. S. Bhaskar, "An experimental estimation of hybrid ANFIS–PSO-based MPPT for PV grid integration under fluctuating sun irradiance," *IEEE Syst. J.*, vol. 14, no. 1, pp. 1218–1229, Mar. 2020.
[29] V. P. Ta and X. K. Dang, "An innovative recurrent cerebellar model articulation controller for piezo-driven micro-motion stage," *Int. J. Innov. Comput., Inf., Control*, vol. 14, no. 4, pp. 1527–1535, 2018.
[30] C. Wu and X. Zhao, "Quantized dynamic output feedback control and $L_2$-gain analysis for networked control systems: A hybrid approach," *IEEE Trans. Netw. Sci. Eng.*, vol. 8, no. 1, pp. 575–587, Jan./Mar. 2021.
[31] W. Ren and J. Xiong, "Lyapunov conditions for input-to-state stability of hybrid systems with memory," *IEEE Trans. Autom. Control*, vol. 64, no. 10, pp. 4307–4313, Oct. 2019.
[32] X. K. Dang, H. N. Truong, and V. D. Do, "A path planning control for a vessel dynamic positioning system based on robust adaptive fuzzy strategy," *Automatika*, vol. 63, no. 3, pp. 580–592, Jul. 2022.
[33] B. C. Gerwick, Jr., *Construction of Marine and Offshore Structures*, 3rd ed. San Francisco, CA, USA: Taylor & Francis, 2007.
[34] *SNAME Technical and Research Bul-Letin 5-5A Site Specific Assessment of Jack-up Units*, Soc. Nav. Architects Mar. Eng., New York, NJ, USA, 2012.
[35] Z. Chao, H. Hong, B. Kaiming, and Y. Xueyuan, "Dynamic amplification factors for a system with multiple-degrees-of-freedom," *Earthq. Eng. Eng. Vib.*, vol. 19, no. 2, pp. 363–375, Apr. 2020.
[36] T. I. Fossen, *Handbook of Marine Craft Hydrodynamics and Motion Control*. Trondheim, Norway: Norwegian Univ. Science Technology, 2011.
[37] M. Zhang, Z. J. Zhang, L. L. Shi, P. Gao, J. B. Zhang, and W. M. Zhang, "A new assembly error modeling and calculating method of complex multi-stage gear transmission system for a large space manipulator," *Mechanism Mach. Theory*, vol. 153, pp. 1–23, Nov. 2020.
[38] V. D. Do, X. K. Dang, T. L. Huynh, and V. C. Ho, "Optimized multi-cascade fuzzy model for ship dynamic positioning system based on genetic algorithm," in *Proc. Int. Conf. Ind. Netw. Intell. Syst.*, 2019, pp. 165–181.
[39] L.-X. Wang and J. M. Mendel, "Fuzzy basis functions, universal approximation, and orthogonal least-squares learning," *IEEE Trans. Neural Netw.*, vol. 3, no. 5, pp. 807–814, Sep. 1992.
[40] V.-D. Do and X.-K. Dang, "The fuzzy particle swarm optimization algorithm design for dynamic positioning system under unexpected impacts," *J. Mech. Eng. Sci.*, vol. 13, no. 3, pp. 5407–5423, Sep. 2019.
[41] A. C. Elizalde and P. Goldsmith, "Adaptive fuzzy-Lyapunov controller using biologically inspired swarm intelligence," *Appl. Bionics Biomech.*, vol. 5, no. 1, pp. 33–46, 2008.
[42] G. Yu, J. Sun, Z. Wu, H. Liu, and W. Ji, "Research on a multi-motor coordinated control strategy based on fuzzy ring coupling control," in *Proc. Chin. Automat. Congr. (CAC)*, 2020, pp. 7068–7072.

**XUAN-KIEN DANG** (Member, IEEE) was born in Haiphong, Vietnam, in 1978. He received the Ph.D. degree in control science and engineering from the Huazhong University of Science and Technology, China, in June 2012. He is currently working as the Director of the Graduate School, Ho Chi Minh City University of Transport, Vietnam, where he is also a Researcher with the Artificial Intelligent in Transportation (AIT). His current research interests include control theory, automation, maritime technology, underwater vehicles, optimal and robust control, and networked control systems. He has been awarded the Best Paper Award in the Fourth Conference of Science and Technology, Ho Chi Minh City University of Transport, in 2018, the President Prize for Award Winner of The Excellent Paper of The 17th Asia Maritime & Fisheries Universities Forum, in 2018, and the Doctoral Scholarship from the Huazhong University of Science and Technology, from 2008 to 2012.

**TIEN-DAT TRAN** (Member, IEEE) was born in Haiphong, Vietnam, in 1979. He received the master's degree from Vietnam Maritime University, in 2008. He is currently pursuing the Ph.D. degree with the Graduate School, Ho Chi Minh City University of Transport, Vietnam. He is also a Researcher at Artificial Intelligent in Transportation (AIT), Ho Chi Minh City University of Transport, where he is also a Lecturer with the Faculty of Mechanical Engineering. His current research interests include control theory, automation, maritime technology, underwater vehicles, and offshore engineering.

**VIET-DUNG DO** (Member, IEEE) was born in Ho Chi Minh City, Vietnam, in 1987. He received the master's degree in control theory and automation from the Ho Chi Minh City University of Transport, in 2016, where he is currently pursuing the Ph.D. degree with the Graduate School. He is also working as the Dean of the Faculty of Electrical and Electronic Engineering, Dong An Polytechnic, Vietnam, and a Researcher at Artificial Intelligent in Transportation (AIT), Ho Chi Minh City University of Transport. His current research interests include control theory, automation, maritime technology, underwater vehicles, and optimal and robust control. He had been awarded the President Prize for Award Winner of The Excellent Paper of the 17th Asia Maritime & Fisheries Universities Forum, in 2018.

**LE ANH-HOANG HO** received the master's degree in automation and control engineering from the Ho Chi Minh City University of Transport, Vietnam, in 2018. He is currently a Lecturer with Van Hien University, Vietnam, and a Researcher at Artificial Intelligent in Transportation (AIT), Ho Chi Minh City University of Transport. His research interests include control theory, automation, the Internet of Things, and artificial intelligence.

**VAN-VANG LE** was born in Haiphong, Vietnam, in 1965. He received the Ph.D. degree in machinery and equipment in Russia, in 2010. He is currently working as the Vice President of the Ho Chi Minh City University of Transport, Vietnam, where he is also a Researcher at Artificial Intelligent in Transportation (AIT). His current research interests include maritime technology, underwater vehicles, ship machinery and equipment, and offshore engineering.



View publication stats